Analyst

PAPER

View Article Online
View Journal | View Issue

Cite this: *Analyst*, 2015, **140**, 5162

Label-free identification and characterization of living human primary and secondary tumour cells

Dimitrios Tsikritsis,[a] Susanna Richmond,[b] Patrick Stewart,[c] Alistair Elfick[a] and Andrew Downes*[a]

Received 29th April 2015,
Accepted 5th June 2015

DOI: 10.1039/c5an00851d

www.rsc.org/analyst

We used three label-free minimally invasive methods to characterize individual cells derived from primary and secondary tumours from the same patient, and of the same type – colorectal. Raman spectroscopy distinguished cells by their biochemical 'fingerprint' in a vibrational spectrum with 100% accuracy, and revealed that the primary cell line contains more lipids and alpha-helix proteins, whereas the secondary cell line contains more porphyrins and beta-sheet proteins. Stimulated Raman scattering (SRS) microscopy distinguished cells in chemically-specific images of CH_2 bonds which revealed lipid droplets in secondary tumour cells. Atomic force microscopy (AFM) was used to distinguish cells with 80% accuracy by measuring their elasticity – secondary tumour cells (SW620) are around 3 times softer than primary ones (SW480). As well as characterizing the physical and biochemical differences between cell lines *in vitro*, these techniques offer three novel methods which could potentially be used for diagnosis – to assign a tumour as primary or secondary.

1. Introduction

Metastasis – the spreading of cancer from one organ to another – results in secondary tumours which are responsible for 90% of deaths from cancer.[1] To reduce death rates, it is essential to understand metastasis and characterize primary and secondary tumours. Primary tumours possess different genetic profiles[2,3] from secondary tumours, so this is used to clinically diagnose whether a tumour is primary or secondary in nature.

Receptor biomarkers are specific to a cancer type,[4] and these biomarkers of a secondary tumour should remain unchanged from the primary source. Alternatively, some biomarkers may be specific to metastasis.[5] So, in future it may be possible to distinguish primary and secondary tumours with MRI or CT contrast agents, such as nanoparticles coated with such antibodies.

However, there is currently no label-free method to distinguish primary from secondary tumours. Label-free methods which are real time would improve treatment over genetic tests, as they would be performed during surgery *in vivo* or on excised tissue. As well as being directly relevant to optimum patient treatment, such label-free methods may also offer an improvement in understanding the mechanism of metastasis.

Raman spectroscopy[6] is a form of optical spectroscopy which does not require labels like fluorophores. A well-defined laser frequency excites vibrational bonds in biomolecules (such as C–C, C–H, C═O). A small proportion of the laser light is absorbed by the molecule, then re-emitted at a lower frequency. The frequency shift of the light is equal to the frequency of the molecular vibration. When the scattered light is passed through a spectrometer, a spectrum of peaks occurs at characteristic frequency shifts which correspond to the vibrational bonds. This won C.V. Raman the Nobel prize in 1930. The technique is applicable to individual living cells[7,8] by focussing the laser within a microscope, and the Raman spectrum can be considered as a biochemical fingerprint of the cell. Raman spectroscopy has been successfully applied to cancer cells and tissues to distinguish between cancerous and healthy tissue or cells.[9–15]

Raman spectroscopy has also been applied to the study of metastasis in several ways. Firstly, cells or tissue from a primary tumour are compared with a metastatic tumour spread to a different organ.[16] Secondly, unrelated cell lines which cause metastasis are compared with those which do not.[17,18] Thirdly, different patients with either a primary or secondary tumour have been compared.[19] Fourthly, primary tumours were compared between patients who went on to develop metastasis with those who did not.[20] Finally, Raman spectroscopy has distinguished between benign, primary

[a]*Institute for BioEngineering, University of Edinburgh, UK. Fax: +44 (0)131 650 6551; Tel: +44 (0)131 650 5660*
[b]*School of Physics, University of Edinburgh, UK*
[c]*School of Engineering, University of Edinburgh, UK*

and secondary malignancies in lymph nodes from a variety of patients.[21] Until now, there has not been a Raman comparison of primary (non-metastatic) and secondary (metastatic) tumour cells from the same organ and the same patient, such as those in this study. This is crucial to separating out the single difference – the primary or secondary nature of the tumour cells – from other variations such as organ, or person.

Atomic Force Microscopy (AFM)[22,23] is a technique for nanoscale topographic profiling of a surface, using a cantilever with a tip of radius ~10 nm. However, it can also be used to measure the Elasticity (Young's modulus) of a compressible surface.[24] It was first applied to cancer as a comparison of cell elasticity between metastatic and healthy cells.[25,26] It has since been extended to staging the disease in mice breast tissue as early, normal, benign, or invasive; and for comparison of primary breast *vs.* metastatic lung tissue in mice.[27] AFM has also compared low and highly metastatic cells *in vitro*.[28,29] The technique measures lower average values of elasticity for metastatic cells,[27] and for those with high potential for metastasis.[28,29] Until now, there has been no comparison of primary (non-metastatic) and secondary (metastatic) tumour cell lines from the same organ and the same patient, and no quantitative measure of the accuracy of AFM to assign cells as metastatic or non-metastatic.

Raman *microscopy* can be performed by raster scanning a sample and acquiring a Raman spectrum at each pixel, but is slow – around 2 seconds per pixel.[30] It has been applied to cancer tissue to characterize regions, such as Basal Cell Carcinoma in skin,[11,30] and malignant from normal lung tissue.[31] However, far more rapid versions of Raman microscopy exist which exploit multi-photon excitation, namely coherent anti-Stokes Raman scattering (CARS) microscopy[32] and stimulated Raman scattering (SRS) microscopy[33] which is considered as an improvement over CARS microscopy due to its background- and artefact-free images. CARS has been used to identify regions as cancerous – offering label-free versions of Haematoxylin and Eosin stains with excellent correlation.[34,35] CARS has also been used to investigate metastatic cells – measuring uptake of lipids,[36] and observing them in the bloodstream due to their higher lipid content.[37] SRS has been applied to imaging cancer tissue,[38] and successfully identified tumour margins by imaging symmetric and anti-symmetric CH_2 vibrations (at 2845 cm^{-1} and 2930 cm^{-1} respectively). It has also been applied to a primary brain tumour and its metastasis into breast tissue,[38] but there was no clear difference between images.

AFM, Raman spectroscopy, and SRS microscopy are all techniques which are able to distinguish cancerous from healthy cells and tissue. So all these techniques will be applied to primary and secondary cancer cells in this study, to determine their effectiveness. To distinguish only between the primary and secondary nature of the cells, rather than any other differences, we used the colorectal cell lines SW480 (primary) and SW620 (secondary). This crucially removes any differences related to tumour environment (organ). This pair of cell lines is also from the same patient, so any differences will strictly be attributed solely to their primary or secondary nature.[39]

2. Materials and methods

2.1 Cell culture

SW480 and SW620 cell lines were acquired from the American Type Culture Collection (ATCC), and have both been cultured for less than 6 months. They were both cultured in Dulbecco's Modified Eagle Medium (Gibco 41966), supplemented with 10% Foetal Calf Serum (Gibco 16140) without antibiotics. Cells were plated onto glass-bottom dishes (WPI Fluorodish FD35) for stimulated Raman scattering (SRS) microscopy and atomic force microscopy (AFM), and onto 0.15–0.18 mm thick quartz substrates (SPI supplies 1019T-AB) for Raman spectroscopy. For SRS fresh media was added, but for AFM and Raman spectroscopy the media was replaced by Phosphate Buffer Saline which maintained cell viability during measurements.

Oil red O (Sigma O0625) was dissolved in isopropanol, filtered and diluted to 60% working solution with distilled water. Cells were fixed with 10% formaldehyde (Sigma 47608) for 20 minutes at room temperature and washed twice with PBS. Lipid droplets were stained by adding Oil red O working solution for 15 minutes at room temperature, followed by 2 washing steps with distilled water.

2.2 Atomic force microscopy (AFM)

We used an AFM (Bruker Bioscope II) on an inverted microscope, with a 20× phase contrast objective lens to view cells and the AFM cantilever tip. A soft cantilever (Bruker MLCT) was mounted into the AFM, and its sensitivity measured on a glass substrate in air, enabling measurement of the cantilever tip upward deflection as a known distance in nanometres. The tip was then retracted from the surface, and a power spectrum measured using a software module. The area under the fundamental vibrational mode of the cantilever was equated to the thermal energy to deduce the cantilever stiffness, k_c. This enables measurement of the repulsive force, F, experienced by the cantilever tip by calibrating according to the equation $F = k_c Z_2$, where Z_2 is the upward deflection of the cantilever tip. Living adherent cells were located and the tip apex positioned above the centre of the nucleus. A 'force–distance' curve was then measured by indenting until the force reaches a given trigger value to avoid damage. The 'distance' is the movement of the fixed end of the cantilever, Z_1. The indentation depth of the tip apex into the cell, $\delta = Z_1 - Z_2$, where Z_1 was known and Z_2 was deduced using $F = k_c Z_2$.

The cell Elasticity (E), or Young's Modulus, is extracted using the Hertz model for a spherical-ended indenter, $F = 4/(3[1 - \nu^2])ER^{1/2}\delta^{3/2}$ where R is the AFM tip radius (taken as 20 nm for these probes), and ν is the Poisson's ratio – a measure of compressibility – taken as 0.37. The Poisson's ratio of living cells was measured as 0.36–0.38,[40] and 0.37.[41] AFM data was fitted to this Hertz model using the open source software, AtomicJ.[42] Both indentation and retraction Force–distance curves were acquired sequentially for the same cell.

2.3 Raman spectroscopy

We used a Renishaw InVia Raman microspectroscopy system, which focusses laser light of wavelength 785 nm into a spot of

approximate size (FWHM) 2 μm laterally and 20 μm axially, by under-filling a 0.75 NA phase contrast objective lens (Leica HCX PL FL 40×/0.75 PH2). The spectral resolution of the Raman system was measured as 7 cm^{-1} (FWHM). Raman spectra were acquired from adherent cells with the laser spot focussed at the boundary between cytoplasm and nucleus. To improve the signal to noise ratio, each spectrum was acquired for 8× 300 s with a laser power of 40 mW measured at the sample. We acquired phase contrast images before and after Raman spectroscopy, and observed no changes to the cells. A background spectrum was acquired by displacing the sample to a nearby region of bare substrate with no cells, then this spectrum subtracted from the spectrum of the cell. This removes the large background signal of the quartz substrate from the cell spectrum. The laser spot was focussed 2 μm above the substrate, and this height was not changed while all cell spectra and background spectra were acquired.

Each spectrum was then processed in several ways: they were first flattened to remove the effect of cellular autofluorescence[43] using the small-window moving average automated baseline correction (SWiMA) procedure. The Matlab code was kindly provided by the author Schulze. The flattening procedure iteratively applies a small, but increasing, moving average window in conjunction with peak stripping to estimate spectral baselines. Then cosmic ray spikes were removed if present, using a further automated algorithm by Schulze.[44] In this cosmic ray removal algorithm, individual Raman spectra from one group (primary or secondary) are compared with each other. When pixel values (Raman intensities at a given wavenumber) are more than 3 standard deviations above the mean, the value is truncated. This process is repeated until the pixel value is less than 3 standard deviations above the mean. Resulting spectra were flattened once more with the same procedure, in case the first flattening procedure was performed on a spectrum with a cosmic ray. Finally, the maximum intensity – highest peak in the spectrum – was normalized to unity. Once processed, principal component analysis (PCA) was performed on an equal number of cells (16 for each group). Each spectrum can be expressed as a linear combination of other principal component spectra, αPC1 + βPC2 + γPC3...., and the scores α and β were plotted on a scatter plot, in order to separate out the two groups of cells.

2.4 Stimulated Raman scattering (SRS) microscopy

We employed a home-built multi-photon microscopy system[45] adapted for SRS microscopy. This adaptation consists of the addition of an amplitude modulator (New Focus 4103-01) at 5 MHz to the Stokes beam, and a lock-in amplifier (Stanford Research SR844) to the detection of transmitted pump beam.

We used 30 mW of each beam, measured at the sample, delivered by a water-immersion multi-photon objective lens of numerical aperture 1.05 (Olympus XLPlan N). The resolution of the system was previously measured as 250 nm FWHM laterally and 1.1 μm FWHM axially.[34] Stacks of 10 images were acquired at 1 μm separation, and converted into a 2-dimensional image by *Z*-projection at maximum intensity to observe all the lipid droplets throughout the cell. Images had a 61 μs pixel dwell time, consisted of 512 × 512 pixels, and were averaged 10 times to enhance quality.

3. Results and discussion

3.1 Atomic force microscopy (AFM)

Elasticity values were deduced for a total number of 56 primary cells (SW480) and 45 secondary cells (SW620), and are plotted in a histogram in Fig. 1. We found the mean values and standard deviations of elasticity to be 1.39 ± 0.71 kPa (SW480 retrace) and 0.834 ± 1.43 kPa (SW620 retrace), using the retraction part of the force–distance curve. Median values of 1.26 kPa (SW480 retrace) and 0.406 kPa (SW620 retrace) remove the outliers to offer more representative values for the cell types, and show that the secondary cells are three times softer than primary cells. We performed Welch's *t*-test on these elasticity values to determine the likelihood of the null hypothesis, that both cell types have the same elasticity. This was rejected and was found to be statistically significant [p = 0.0197]. SW480 cells were previously measured to have an elasticity of 0.47 kPa,[46] using a tipless cantilever and a model of the cell as an ellipsoid to extract the elasticity, but no comparison was made with SW620 cells. Uncertainty in the AFM cantilever's tip radius R, nominally taken as 20 nm from manufacturer's data for the Hertz model, will result in values which are not absolutely accurate, but relatively accurate when using the same probe – as was the case in this study. For absolute values of elasticity, a calibration sample is required. 46 of 56 measurements on primary cells have an elasticity greater than a threshold of 0.70 kPa, and 35 of 45 secondary cells have an elasticity below this threshold. This corresponds to an accuracy of 80% for discriminating cell type by elasticity.

These results compare favourably with previous AFM measurements which show secondary tumours have lower elasticities (*i.e.* are softer) than primary tumours from different

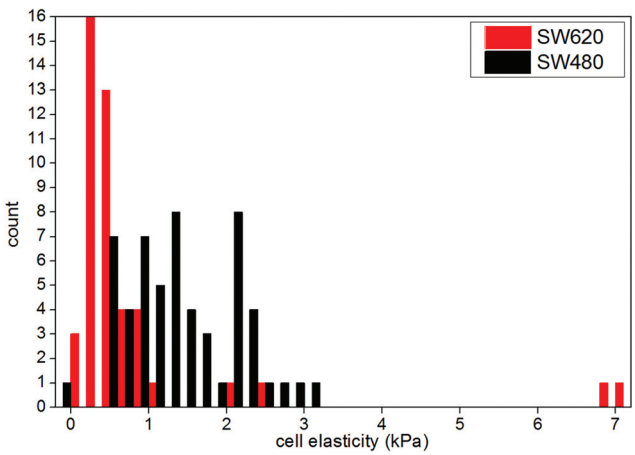

Fig. 1 Histogram of cell elasticity for primary (SW480) and secondary (SW620) cancer cells.

mice,[47] and that cells with a high metastatic potential have lower average elasticities than cells with low metastatic potential.[28,29] However, we are the first to compare primary and secondary cells from the same organ, or from the same patient. We are also the first to give a quantitative measure of the accuracy of discriminating cell types by this AFM mechanical measurement.

3.2 Raman spectroscopy

Raman spectra were acquired on 16 individual cells of each type, SW480 and SW620. The average spectrum for each type, plotted in Fig. 2, shows significant changes. The difference spectrum (SW620 minus SW480) highlights the biochemical differences between the two cell types. These biochemical differences are presented in Table 1, according to assignment of the peaks in the Raman spectrum to classes of biomolecule.[48] Broadly speaking, these suggest that the SW620 cells contain a higher proportion of porphyrins and beta-sheet proteins than SW480 cells, and SW480s contain a higher proportion of lipids and alpha-helix proteins than SW620s. The increased concentration of porphyrins in tumours was first revealed in 1923 [49] and these molecules are also autofluorescent in the red part of the spectrum so can be detected by imaging.[50] We also compared unnormalised spectra, which showed similar spectral differences and essentially the same biochemical differences as those presented in Fig. 2 and Table 1. Ratios of normalised or unnormalised spectra also demonstrated the same positive and negative peaks as those in Fig. 2 and Table 1.

Principal Component Analysis (PCA) was used to see how well individual cells could be distinguished by Raman spectroscopy. PCA reduces the differences in spectra between all 32 cells in the study, to just two variables. In Fig. 3, each spectrum from an individual cell is plotted as a separate data point. It is clear that all the cells could be identified clearly as SW480 or SW620 just by noting their position on the plot. When an unknown cell is probed by Raman spectroscopy, it can be plotted onto the same figure and easily characterized as SW480 or SW620, with an accuracy approaching 100%. When we randomly selected 11 of each cell type to create a training set, the remaining 10 cells were used as a test set and were all correctly identified when superimposed onto the training set PCA plot, with the resulting plot appearing very similar to Fig. 3.

The only other Raman study to compare metastatic and non-metastatic cell lines was performed over the range 2820–3030 cm^{-1}, which is populated only by C–H bonds, and only produced partial discrimination using PCA.[17]

Table 1 Assignment of vibrational modes[48] in the difference Raman spectrum in Fig. 2

Raman frequency (wavenumbers, cm^{-1})	Biomolecules more abundant in SW480
621	Phenylalanine
642	Phenylalanine
854	Phenylalanine
1002	Phenylalanine
1031	Phenylalanine
1445	Lipids
1660	α-helix proteins
Raman frequency (wavenumbers, cm^{-1})	**Biomolecules more abundant in SW620**
752	Porphyrins
1520	Porphyrins
1551	Porphyrins
1622	Porphyrins
1676	β-sheet proteins

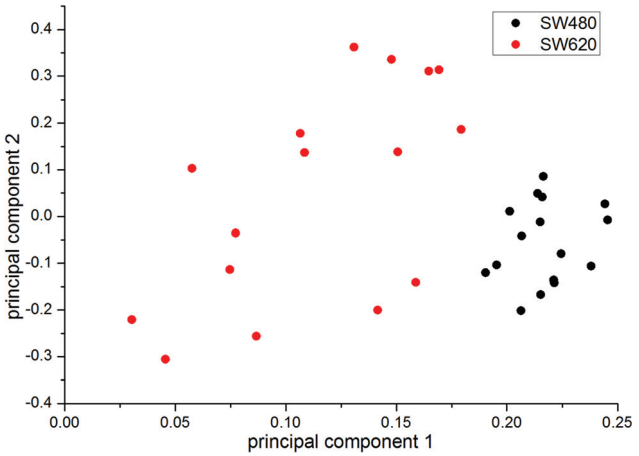

Fig. 3 Principal Component Analysis (PCA) plot of Raman spectra for 16 individual cells of each type (SW480 in black, SW620 in red). Clear separation is observed between the two groups, demonstrating the effectiveness of Raman spectroscopy to characterize unknown cells as one or other type.

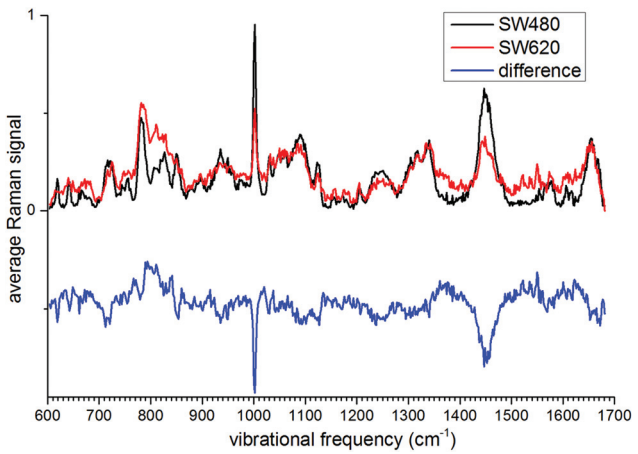

Fig. 2 Average Raman spectra for primary (SW480) and secondary (SW620) cell lines. The difference spectrum (offset for clarity) is the spectrum for SW620 minus the spectrum for SW480.

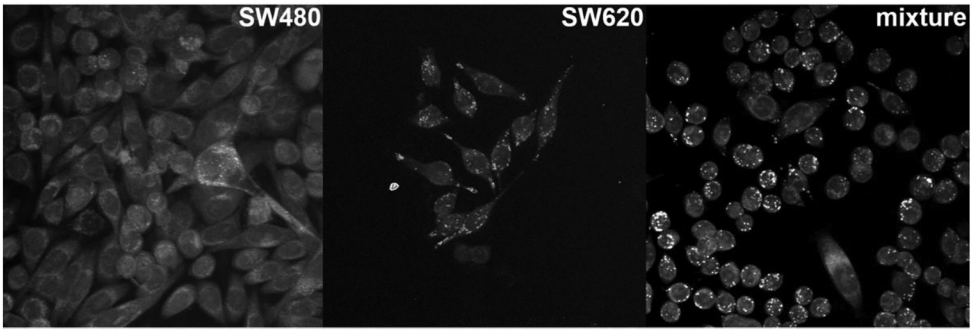

Fig. 4 Stimulated Raman Scattering (SRS) images, acquired at a frequency of 2930 cm^{-1} (specific to the CH_2 anti-symmetric stretch, dominated by lipids). All three images are maximum intensity *Z*-projections, from volume stacks of size 200 × 200 × 10 μm into two-dimensional images of size 200 × 200 μm.

3.3 Stimulated Raman scattering (SRS) microscopy

We performed SRS microscopy to image the concentration of CH_2 groups, and imaged three types of sample in Fig. 4. As well as the purely SW480 and SW620 samples, we also imaged a mixture of these cell types plated the previous day. Images of CH_2 bonds are dominated by lipids due to the high proportion of these groups in lipids, compared to other biomolecules. The SW480s are usually larger than the SW620s, and can be seen in the mixed sample both due to their size and the far smaller number of lipid droplets.

Combining the results of Raman spectroscopy and SRS microscopy, we deduced that although the SW480 cells have a higher proportion of lipids in than SW620 cells, there are more lipid droplets – which are predominantly triglycerides[51] – in the SW620 cells. This is supported by a previous observation that there is a dramatic increase in the amount of triglycerides in SW620 compared to SW480 cells.[52] The only Raman study of metastatic and non-metastatic cell lines[17] was inconclusive about the amount and type of lipids in metastatic cells, but suggested a higher likelihood of lipid droplets in stained metastatic cells. The relative abundances of lipid droplets in both cell types is confirmed by Oil red O staining of fixed cells in Fig. 5.

4. Conclusion

Three techniques were presented for analysis of living human primary and secondary tumour cells. All techniques are label-free, non-destructive and applied to individual cells. Crucially, SW480 and SW620 cell lines are from the same patient and the same organ. This removed all unwanted variations and revealing only the primary or secondary nature of the cells. All other comparisons either involve different organs, different patients, or unrelated cell lines.

A good deal of physical and biochemical information was revealed about the differences between primary & secondary cells. This assumes that the differences observed for one patient, are also observed for other patients, and that differences between cells *in vitro* are observed in tissue samples. Further work is required to prove this. Secondary (metastatic) cells are softer, are smaller, have far more porphyrins and lipid droplets, but have a lower proportion of lipids and structural proteins than primary tumour cells.

We also distinguished between cell types using these three analytical methods, enabling all three techniques as methods for diagnosis in humans of primary or secondary tumour. All techniques can be applied to excised tissue from surgery, to

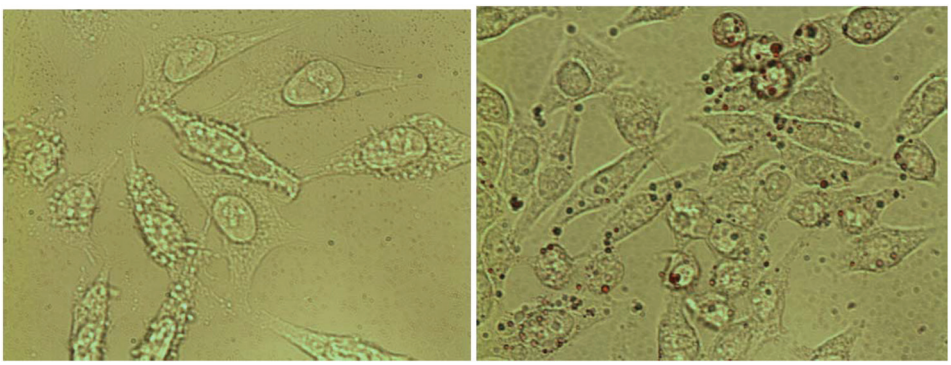

Fig. 5 Transmitted light images of primary (SW480, left) and secondary (SW620, right) tumour cells stained with the lipophilic dye, Oil red O. Red staining confirms the presence of high levels of lipid droplets in the secondary tumour cells. Image sizes are 120 × 90 μm.

biopsy or fine needle aspirates, or modified to application *in vivo* during surgery – without the requirement to fix, slice, treat or stain the sample. SRS microscopy and Raman spectroscopy can also be used *in vivo* beneath the surface of tissue.

Acknowledgements

Dimitrios Tsikritsis has a PhD studentship which is funded by the EPSRC. We would like to thank Rabah Mouras for advice on SRS microscopy and AFM. No potential conflicts of interest were disclosed. There are no financial disclosures from any authors.

References

1 C. L. Chaffer and R. A. Weinberg, A Perspective on Cancer Cell Metastasis, *Science*, 2011, **331**, 1559–1564.
2 A. Fishman, E. Shalom-Paz, M. Fejgin, E. Gaber, M. Altaras and A. Amiel, Comparing the genetic changes detected in the primary and secondary tumor sites of ovarian cancer using comparative genomic hybridization, *Int. J. Gynecol. Cancer*, 2005, **15**, 261–266.
3 S. Noguchi, K. Motomura, H. Inaji, S. Imaoka and H. Koyama, Differentiation of primary and secondary breast cancer with clonal analysis, *Surgery*, 1994, **115**, 458–462.
4 M. T. Weigel and M. Dowsett, Current and emerging biomarkers in breast cancer: prognosis and prediction, *Endocr.-Relat. Cancer*, 2010, **17**, R245–R262.
5 K. Sukhdeo, R. I. Paramban, J. G. Vidal, J. Elia, J. Martin, M. Rivera, D. R. Carrasco, A. Jarrar, M. F. Kalady, C. T. Carson, R. Balderas, A. B. Hjelmeland, J. D. Lathia and J. N. Rich, Multiplex Flow Cytometry Barcoding and Antibody Arrays Identify Surface Antigen Profiles of Primary and Metastatic Colon Cancer Cell Lines, *PLoS One*, 2013, **8**, e53015.
6 C. V. Raman and K. S. Krishnan, A New Type of Secondary Radiation, *Nature*, 1928, **121**, 501–502.
7 I. Notingher, S. Verrier, H. Romanska, A. E. Bishop, J. M. Polak and L. L. Hench, In situ characterisation of living cells by Raman spectroscopy, *Spectroscopy*, 2002, **16**, 43–51.
8 A. Downes and A. Elfick, Raman Spectroscopy and Related Techniques in Biomedicine, *Sensors*, 2010, **10**, 1871–1889.
9 R. Thomas, K. A. Bakeev, M. Claybourn and R. Chimenti, The Use of Raman Spectroscopy in Cancer Diagnostics, *Spectroscopy*, 2013, **28**, 36–43.
10 A. Mahadevan-Jansen and R. Richards-Kortum, Raman spectroscopy for cancer detection: a review, in *Engineering in Medicine and Biology Society, Proceedings of the 19th Annual International Conference of the IEEE, 1997, IEEE*, 1997, 2722–2728.
11 A. Nijssen, T. C. Bakker Schut, F. Heule, P. J. Caspers, D. P. Hayes, M. H. A. Neumann and G. J. Puppels, Discriminating Basal Cell Carcinoma from its Surrounding Tissue by Raman Spectroscopy, *J. Invest. Dermatol.*, 2002, **119**, 64–69.
12 P. Caspers, G. Lucassen and G. Puppels, Combined in vivo confocal Raman spectroscopy and confocal microscopy of human skin, *Biophys. J.*, 2003, **85**, 572–580.
13 C. Kendall, M. Isabelle, F. Bazant-Hegemark, J. Hutchings, L. Orr, J. Babrah, R. Baker and N. Stone, Vibrational spectroscopy: a clinical tool for cancer diagnostics, *Analyst*, 2009, **134**, 1029–1045.
14 A. S. Haka, K. E. Shafer-Peltier, M. Fitzmaurice, J. Crowe, R. R. Dasari and M. S. Feld, Diagnosing breast cancer by using Raman spectroscopy, *Proc. Natl. Acad. Sci. U. S. A.*, 2005, **102**, 12371–12376.
15 M. D. Keller, E. M. Kanter and A. Mahadevan-Jansen, Raman Spectroscopy for Cancer Diagnosis, *Spectroscopy*, 2006, 21.
16 N. Santana, C. Nieva, A. Sierra, M. Marro, S. Rao and D. Petrov, Raman microspectroscopy is a tool to identify the metastatic ability of breast tumors, in *BioPhotonics*, 2011 International Workshop on, 2011, 1–3.
17 C. Nieva, M. Marro, N. Santana-Codina, S. Rao, D. Petrov and A. Sierra, The Lipid Phenotype of Breast Cancer Cells Characterized by Raman Microspectroscopy: Towards a Stratification of Malignancy, *PLoS One*, 2012, **7**, e46456.
18 M. Hedegaard, C. Krafft, H. J. Ditzel, L. E. Johansen, S. Hassing and J. Popp, Discriminating isogenic cancer cells and identifying altered unsaturated fatty acid content as associated with metastasis status, using k-means clustering and partial least squares-discriminant analysis of Raman maps, *Anal. Chem.*, 2010, **82**, 2797–2802.
19 A. F. d. Oliveira, I. D. d. A. O. Santos, S. B. Cartaxo, R. A. Bitar, M. M. S. e. S. Enokihara, H. d. S. Martinho, A. A. Martin and L. M. Ferreira, Differential diagnosis in primary and metastatic cutaneous melanoma by FT-Raman spectroscopy, *Acta Cirurgica Brasileira*, 2010, **25**, 434–439.
20 M. Tollefson, J. Magera, T. Sebo, J. Cohen, A. Drauch, J. Maier and I. Frank, Raman spectral imaging of prostate cancer: can Raman molecular imaging be used to augment standard histopathology?, *BJU Int.*, 2010, **106**, 484–488.
21 G. R. Lloyd, L. E. Orr, J. Christie-Brown, K. McCarthy, S. Rose, M. Thomas and N. Stone, Discrimination between benign, primary and secondary malignancies in lymph nodes from the head and neck utilising Raman spectroscopy and multivariate analysis, *Analyst*, 2013, **138**, 3900–3908.
22 G. Binnig, C. F. Quate and C. Gerber, Atomic Force Microscope, *Phys. Rev. Lett.*, 1986, **56**, 930–933.
23 M. Radmacher, R. Tillamnn, M. Fritz and H. Gaub, From molecules to cells: imaging soft samples with the atomic force microscope, *Science*, 1992, **257**, 1900–1905.
24 J. Domke and M. Radmacher, Measuring the Elastic Properties of Thin Polymer Films with the Atomic Force Microscope, *Langmuir*, 1998, **14**, 3320–3325.
25 E. C. Sarah, J. Yu-Sheng, T. Julianne, W. Roger, R. JianYu and K. G. James, AFM-based analysis of human metastatic cancer cells, *Nanotechnology*, 2008, **19**, 384003.

26 S. E. Cross, Y.-S. Jin, J. Rao and J. K. Gimzewski, Nanomechanical analysis of cells from cancer patients, *Nat Nanotechnol.*, 2007, **2**, 780–783.
27 M. Plodinec, M. Loparic, C. A. Monnier, E. C. Obermann, R. Zanetti-Dallenbach, P. Oertle, J. T. Hyotyla, U. Aebi, M. Bentires-Alj, Y. H. LimRoderick and C.-A. Schoenenberger, The nanomechanical signature of breast cancer, *Nat Nanotechnol.*, 2012, **7**, 757–765.
28 W. Xu, R. Mezencev, B. Kim, L. Wang, J. McDonald and T. Sulchek, Cell stiffness is a biomarker of the metastatic potential of ovarian cancer cells, *PLoS one*, 2012, **7**, e46609.
29 Z. Zhou, C. Zheng, S. Li, X. Zhou, Z. Liu, Q. He, N. Zhang, A. Ngan, B. Tang and A. Wang, AFM nanoindentation detection of the elastic modulus of tongue squamous carcinoma cells with different metastatic potentials, *Nanomedicine*, 2013, **9**, 864–874.
30 K. Kong, C. J. Rowlands, S. Varma, W. Perkins, I. H. Leach, A. A. Koloydenko, H. C. Williams and I. Notingher, Diagnosis of tumors during tissue-conserving surgery with integrated autofluorescence and Raman scattering microscopy, *Proc. Natl. Acad. Sci. U. S. A.*, 2013, **110**, 15189–15194.
31 N. D. Magee, J. R. Beattie, C. Carland, K. McManus, I. Bradbury, D. A. Fennell, M. Ennis, J. J. McGarvey, J. S. Elborn, P. W. Hamilton and R. Davis, Raman microscopy in the diagnosis and prognosis of surgically resected non-small cell lung cancer, *J. Biomed. Opt.*, 2010, **15**, 026015.
32 A. Zumbusch, G. R. Holtom and X. S. Xie, Three-Dimensional Vibrational Imaging by Coherent Anti-Stokes Raman Scattering, *Phys. Rev. Lett.*, 1999, **82**, 4142–4145.
33 C. W. Freudiger, W. Min, B. G. Saar, S. Lu, G. R. Holtom, C. He, J. C. Tsai, J. X. Kang and X. S. Xie, Label-free biomedical imaging with high sensitivity by stimulated Raman scattering microscopy, *Science*, 2008, **322**, 1857–1861.
34 R. Mouras, G. Rischitor, A. Downes, D. Salter and A. Elfick, Nonlinear optical microscopy for drug delivery monitoring and cancer tissue imaging, *J. Raman Spectrosc.*, 2010, **41**, 848–852.
35 R. Mouras, P. Bagnaninchi, A. Downes and A. Elfick, Multimodal, label-free nonlinear optical imaging for applications in biology and biomedical science, *J. Raman Spectrosc.*, 2013, **44**, 1373–1378.
36 T. T. Le, T. B. Huff and J.-X. Cheng, Coherent anti-Stokes Raman scattering imaging of lipids in cancer metastasis, *BMC Cancer*, 2009, **9**, 42.
37 R. Mitra, O. Chao, Y. Urasaki, O. B. Goodman and T. T. Le, Detection of lipid-rich prostate circulating tumour cells with coherent anti-Stokes Raman scattering microscopy, *BMC Cancer*, 2012, **12**, 540.
38 X. S. Xie, C. W. Freudiger, D. A. Orringer, B. G. Saar, M. Ji, Q. Zeng, L. Ottoboni, W. Ying, C. Waeber and J. R. Sims, Multicolored Stain-Free Histopathology with Coherent Raman Imaging, *Lab. Invest.*, 2012, **92**, 1492–1502.
39 R. E. Hewitt, A. McMarlin, D. Kleiner, R. Wersto, P. Martin, M. Tsokos, G. W. Stamp and W. G. Stetler-Stevenson, Validation of a model of colon cancer progression, *J. Pathol.*, 2000, **192**, 446–454.
40 W. R. Trickey, F. P. T. Baaijens, T. A. Laursen, L. G. Alexopoulos and F. Guilak, Determination of the Poisson's ratio of the cell: recovery properties of chondrocytes after release from complete micropipette aspiration, *J. Biomech.*, 2006, **39**, 78–87.
41 D. Shin and K. Athanasiou, Cytoindentation for obtaining cell biomechanical properties, *J. Orthop. Res.*, 1999, **17**, 880–890.
42 P. Hermanowicz, M. Sarna, K. Burda and H. Gabryś, AtomicJ: An open source software for analysis of force curves, *Rev. Sci. Instrum.*, 2014, **85**, 063703.
43 H. G. Schulze, R. B. Foist, K. Okuda, A. Ivanov and R. F. B. Turner, A Small-Window Moving Average-Based Fully Automated Baseline Estimation Method for Raman Spectra, *Appl. Spectrosc.*, 2012, **66**, 757–764.
44 H. G. Schulze and R. F. B. Turner, A Fast, Automated, Polynomial-Based Cosmic Ray Spike Removal Method for the High-Throughput Processing of Raman Spectra, *Appl. Spectrosc.*, 2013, **67**, 457–462.
45 A. Downes, R. Mouras and A. Elfick, A versatile CARS microscope for biological imaging, *J. Raman Spectrosc.*, 2009, **40**, 757–762.
46 O. Jonas, C. T. Mierke and J. A. Kas, Invasive cancer cell lines exhibit biomechanical properties that are distinct from their noninvasive counterparts, *Soft Matter*, 2011, **7**, 11488–11495.
47 M. Plodinec, M. Loparic, C. A. Monnier, E. C. Obermann, R. Zanetti-Dallenbach, P. Oertle, J. T. Hyotyla, U. Aebi, M. Bentires-Alj and R. Y. Lim, The nanomechanical signature of breast cancer, *Nat. Nanotechnol.*, 2012, **7**, 757–765.
48 Z. Movasaghi, S. Rehman and I. U. Rehman, Raman Spectroscopy of Biological Tissues, *Appl. Spectrosc. Rev.*, 2007, **42**, 493–541.
49 A. Policard, A study on the available aspects of experimental tumours examined by Wood's light, *C. R. Seances Soc. Biol. Ses Fil.*, 1924, **91**, 1423–1424.
50 M. Hefti, H. Maximilian Mehdorn, I. Albert and L. Dorner, Fluorescence-Guided Surgery for Malignant Glioma: A Review on Aminolevulinic Acid Induced Protoporphyrin IX Photodynamic Diagnostic in Brain Tumors, *Curr. Med. Imaging Rev.*, 2010, **6**, 254–258.
51 F. Baenke, B. Peck, H. Miess and A. Schulze, Hooked on fat: the role of lipid synthesis in cancer metabolism and tumour development, *Dis. Models & Mech.*, 2013, **6**, 1353–1363.
52 C. J. Fhaner, S. Liu, H. Ji, R. J. Simpson and G. E. Reid, Comprehensive Lipidome Profiling of Isogenic Primary and Metastatic Colon Adenocarcinoma Cell Lines, *Anal. Chem.*, 2012, **84**, 8917–8926.